Appl. Phys. B 74, 653–659 (2002)
DOI: 10.1007/s00340-002-0917-5

Applied Physics B
Lasers and Optics

T.V. DOLGOVA[1]
D. SCHUHMACHER[2]
G. MAROWSKY[2]
A.A. FEDYANIN[1]
O.A. AKTSIPETROV[1,✉]

Second-harmonic interferometric spectroscopy of buried interfaces of column IV semiconductors

[1] Department of Physics, Moscow State University, 119899 Moscow, Russia
[2] Laser-Laboratorium Göttingen, 37077 Göttingen, Germany

Received: 16 October 2001/Revised version: 16 April 2002
Published online: 6 June 2002 •

ABSTRACT The technique of combined optical second-harmonic (SH) intensity and phase spectroscopy, which is the spectroscopic modification of SH phase measurements, is proposed to study the nonlinear optical response of semiconductor interfaces with spectrally close resonant contributions. The spectral dependences of SH intensity and phase from oxidised Si (111) and Ge (111) surfaces are studied in the range of 3.5- to 5-eV SH photon energy. The resonant behaviour of combined SH spectra is associated with a superposition of contributions from direct interband transitions at several critical points of Si and Ge band structures.

PACS 71.20.-b; 73.20.-r; 73.20.At; 78.68.+m; 42.65.-k

1 Introduction

The surfaces of column IV semiconductors such as silicon and germanium have been one of the most intensively studied objects in solid-state physics for decades. Despite tremendous technological progress in silicon and germanium processing, there are still many unresolved fundamental problems concerning dielectric growth and microstructure of Si–SiO_2 and Ge–GeO_2. Although silicon has almost completely displaced germanium in electronic technology, the interest in germanium has recently been revived since Si/Ge alloys have become an important class of semiconductor materials for microelectronic applications. The important issues are electronic excitations at Si–SiO_2 and Ge–GeO_2 interfaces and in Si/Ge films in the limit of ultra-thin (2–10 nm) oxide or alloy films, as well as their relation to electrical defects, including interface traps, fixed oxide charge, trapped oxide charge and mobile ionic charge. Unfortunately, it is not clear to what extent traditional electrical (*C–V, I–V*, etc.) and optical (ellipsometry) methods can be used to study processes in such thin films. For instance, low-frequency *C–V* measurements cannot be taken because of high direct tunnel currents, and the ellipsometric data interpretation is complex for ultra-thin films, since the definition of the dielectric constant becomes ambiguous. On the contrary, optical second-harmonic generation (SHG) spectroscopy capitalising on crystal symmetry has been used successfully for probing strain, defect states, electric fields and electronic transitions at Si–SiO_2 [1–4] and Si–Si_xGe_{1-x} [5] interfaces.

SHG spectroscopy becomes more informative when fundamental or second-harmonic (SH) photon energy is close to the energy of direct electron transitions. These transitions can be either interband or involve interface traps with levels within the band gap. For instance, the variety of interface-state parameters, such as type, density, energy distribution, etc. can be studied by SHG spectroscopy [6, 7]. For interband transitions, the SHG response is enhanced resonantly in the vicinity of specific regions of the band structure, where the combined density of states has a critical (singular) behaviour (Van Hove singularities). The $\chi^{(2)}$ line shape in the spectral vicinity of such a critical point (CP) depends on the dimensionality of the singularity in the dispersion law and influences significantly the resonance parameters, mainly central energies. For the case of Si and Ge, critical points are located close to each other, and the total SHG signal is a superposition of SHG resonances from different CPs. The interference leads to modification of the SHG spectrum. Separating these partial SHG contributions can be complex, due to a large number of adjustable parameters. One of the ways to define the resonance parameters more accurately would be to complement the spectrum of the SH intensity with the SH phase as one more independent characteristic of the SH field.

In this paper combined SH intensity and phase spectroscopy is used to study the resonant SHG response of Si (111)–SiO_2 and Ge (111)–GeO_2 interfaces in the vicinity of several CPs of their band structures in the range of SH photon energy from 3.5 to 5 eV. Two interfering resonant SHG contributions are studied for the Ge (111)–GeO_2 interface. The first is a one-photon resonance of direct transitions near the E_1 CP at the fundamental frequency, and the second is the two-photon resonance in the vicinity of the E_2 CP. A good representation of the combined SHG spectra is provided by two-dimensional (2D) line shapes of the quadratic susceptibility of both resonances. The interference of SHG contributions from two-photon resonances at $E_2(X, \Sigma)$ and E_1' CPs is demonstrated for the Si (111)–SiO_2 interface. Parameters of CPs and line shapes of quadratic susceptibility are derived from a combination of the SH intensity and phase spectra within the simple phenomenological model, which

✉ E-mail: aktsip@shg.ru

takes into account complex Green's function corrections for the SH wave generation along with complex $\chi^{(2)}$.

2 Theory

The SH phase and intensity spectra reflect spectral dependences of optical susceptibilities and Green's function corrections. In the vicinity of resonances it is important to take into consideration all the factors showing critical behaviour both at the fundamental and second-harmonic wavelength. Green's function corrections influence significantly the interference of surface and bulk contributions to the SH field, bringing additional phase shifts as well. Several papers reported a phenomenological description of anisotropic SHG [1, 8, 9]. Transformation of SH polarisation into SH field is described in detail in [10]. Summarising both descriptions, in this section the expressions for SH intensity and phase are derived for (111) surfaces of $m3m$ semiconductors in p-in p-out geometry, taking into account complex Green's function corrections at the fundamental and SH wavelength. Detailed expressions for the anisotropic SH field are presented in the Appendix.

The quadratic polarisation induced inside the medium includes two predominant contributions, i.e. surface and bulk quadrupole terms:

$$\boldsymbol{P}^{(2)\mathrm{S}}(z=+0,2\omega)=\hat{\chi}^{(2),\mathrm{S}}(2\omega):\boldsymbol{E}(\omega)\boldsymbol{E}(\omega), \tag{1}$$

$$\boldsymbol{P}^{(2)\mathrm{Q}}(z,2\omega)=\hat{\chi}^{(2),\mathrm{Q}}(2\omega):\boldsymbol{E}(z,\omega)\nabla\boldsymbol{E}(z,\omega). \tag{2}$$

Since the components of the tensor of the effective surface quadratic susceptibility, $\hat{\chi}^{(2),\mathrm{S}}$, are defined in the surface frame, i.e. in the coordinate frame determined with respect to the surface plane, the surface polarisation, $\boldsymbol{P}^{(2)\mathrm{S}}(2\omega)$, and the vector of the fundamental field, $\boldsymbol{E}(\omega)$, in (1) should be defined in the surface frame. By analogy, the bulk quadrupole quadratic susceptibility, $\hat{\chi}^{(2),\mathrm{Q}}$, the bulk polarisation, $\boldsymbol{P}^{(2)\mathrm{Q}}(2\omega)$, the wave vector of the fundamental radiation in the medium, $\boldsymbol{k}_2^{\omega}$, and $\boldsymbol{E}(\omega)$ are to be calculated in the crystallographic frame. The definition of the frames is presented in Fig. 1. The z axis is directed into the medium.

The expression for the SH field just above the surface, $\boldsymbol{E}(-0,2\omega)$, is derived in three steps. First, the fundamental field $\boldsymbol{E}(z,\omega)$ is calculated in the medium using the Fresnel factor and the transformation tensors from the laboratory to the surface frame and from the surface to the crystallographic frame, respectively. This takes into account experimental geometry: namely, the angle of incidence and the azimuthal sample position. Second, using a set of nonzero components of $\hat{\chi}^{(2),\mathrm{S}}$ and $\hat{\chi}^{(2),\mathrm{Q}}$, the polarisation vectors $\boldsymbol{P}^{(2)\mathrm{S}}(+0,2\omega)$ and $\boldsymbol{P}^{(2)\mathrm{Q}}(z',2\omega)$ are found in the surface and crystallographic frames and then are transformed to the laboratory frame. Finally, the vector of quadratic polarisation should be convolved with the Green's function tensor for a semi-infinite medium $\hat{G}(z,z')$. The z argument is the point of the field detection that can be assigned to the point just above the surface, $z=-0$, since the factor of propagation in air is trivial. The z' argument is the point of the polarisation generation. Due to translational invariance in the surface plane the dependence on in-plane coordinates is omitted and the expression for the SH field vector can be given in the form:

$$\boldsymbol{E}(-0,2\omega)=-4\pi\left(\tfrac{2\omega}{c}\right)^2 \times\int_0^{\infty}\hat{G}(-0,z')\left[\boldsymbol{P}^{\mathrm{S}}\delta(z'-0)+\boldsymbol{P}^{\mathrm{Q}}(z')\right]\mathrm{d}z'. \tag{3}$$

Using expressions for $\hat{G}(-0,z')$ from [11] listed in the Appendix, the SH field vector in the p-in p-out geometry has the form of a Fourier expansion over the azimuthal angle ψ:

$$\boldsymbol{E}(-0,2\omega)=G_0E_p^2(C_0+C_3\cos 3\psi)\begin{pmatrix}1\\0\\k_x^{2\omega}/k_{2z}^{2\omega}\end{pmatrix}. \tag{4}$$

The coefficient $G_0=2\pi\mathrm{i}k_{2z}^{2\omega}\varepsilon_2^{-1}T_{\omega}^2$ is the effective Green's function correction, consisting of a term coming from the Green's function at 2ω and the Fresnel factor T_{ω} at ω. Figure 2 shows the calculated spectral dependences of squared modulus and phase of G_0 for germanium (solid lines) and for silicon (dashed lines). Fourier amplitudes $C_{0(3)}$ are listed in the Appendix and can be written as:

$$C_{0(3)}=\chi^{(2)}_{\parallel,0(3)}+\frac{k_x^{2\omega}}{k_{2z}^{2\omega}}\chi^{(2)}_{\perp,0(3)}. \tag{5}$$

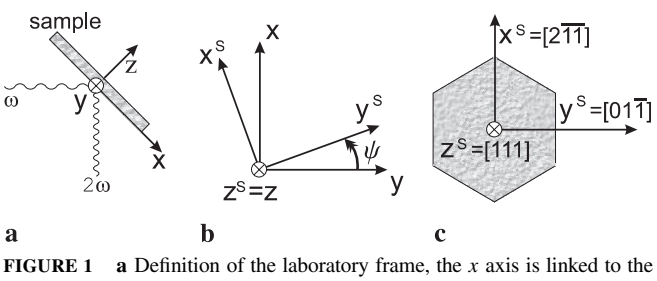

FIGURE 1 **a** Definition of the laboratory frame, the x axis is linked to the incidence plane; **b** relation between laboratory and surface frames, ψ is the azimuthal position of the sample; **c** linkage of the surface frame to directions in the $m3m$ crystal

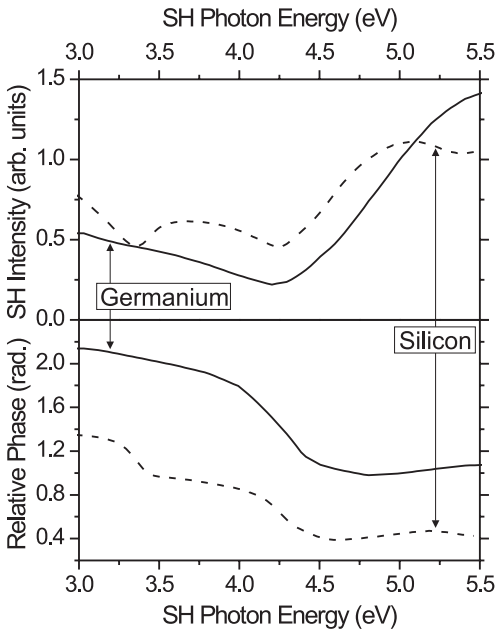

FIGURE 2 Spectral dependences of $|G_0|^2$ and $\arg(G_0)$ calculated for surfaces of germanium (*solid lines*) and silicon (*dashed lines*) using linear dispersion data from [12]

The coefficients $\chi_{\parallel}^{(2)}$ and $\chi_{\perp}^{(2)}$ are the linear combinations of $\chi^{(2),\mathrm{S}}$ and $\chi^{(2),\mathrm{Q}}$ components with nonresonant coefficients depending only on the fundamental wave vector and taking into account the geometry of the nonlinear interaction. The spectral dependence of $\chi_{\perp(\parallel)}^{(2)}$ is a superposition of resonances at $\omega_0 = \omega, 2\omega$ related to several CPs:

$$\chi_{\alpha}^{(2)}(2\omega) = B - \sum_m f_m^{\alpha} \exp\left(\mathrm{i}\phi_m^{\alpha}\right) (\omega_0 - \omega_m + \mathrm{i}\Gamma_m)^n, \qquad (6)$$

where $\alpha = \perp, \parallel$, m enumerates the CP resonances and $n = 1/2, 0, -1/2, -1$ defines the type (dimensionality) of the CP [13]. The oscillator strengths f_m^{α} are supposed to be real numbers. For the sake of simplicity, a slight spectral dependence of the term B including SHG resonances with central energies below 1.5 eV is neglected, and ϕ_m^{α} are integer multiples of $\pi/2$ defining the CP type. The spectra of the squared modulus of the SH field from (4) and of its phase are the values which can be measured by SHG interferometric spectroscopy.

3 Experimental technique

The SHG interferometric spectroscopy setup is shown in Fig. 3. The output of a tunable nanosecond parametric generator/amplifier laser system (Spectra-Physics MOPO 710) is used as a source of the fundamental radiation. The tuning range of the visible OPO branch is 665 nm to 500 nm (1.9 eV to 2.5 eV) and 2 μm to 735 nm (0.6 eV to 1.7 eV) for the idler branch. The pulse duration is 4 ns and the energy is 10 mJ/pulse at a wavelength of 600 nm. The spectral width of the output pulses is approximately 50 cm^{-1} (< 4 nm). A Fresnel rhomb with a Glan prism provides *s*- or *p*-polarised output radiation. A set of lenses is inserted to collimate the beam inside the single-beam interferometric scheme used for SH phase spectroscopy. The 3-mm-thick GG475 filter in the visible OPO range and the 3-mm-thick RG695 plus 3-mm-thick RG715 filters in the OPO idler-wave range remove the residual OPO pump (355 nm) and SHG from the optics of the setup. The reflected SH wave is separated by a set of filters (12 mm of UG5 for the 490- to 520-nm interval, 10 mm of UG5 for 510 to 630 nm, 6 mm of UG11 plus 7 mm of BG3 for 605 to 665 nm and 9 mm of BG39 for 735 to 1000 nm) and detected by a photomultiplier tube and an electronic peak-hold detector. Polarisation of the SH wave is controlled by a Glan prism. The reference channel is used to normalise the SH intensity spectrum over the laser fluence. A slightly wedged *z*-cut quartz plate is used as a source of reference SHG signal, and the detection system is identical to the one in the sample channel. All spectral measurements have to be normalised with the SHG spectrum obtained by measuring two identical quartz samples in signal and reference channels, which takes into account the spectral sensitivity of the optical detection system. The range of the signal wave of the OPO system and the *p*-in, *p*-out polarisation combination are used in the present work.

The SHG interferogram is obtained by translating the reference along the fundamental laser beam, varying the distance l between the phase reference and the sample. It has a cosine shape typical for SH phase measurements:

$$I(l) = I_{\mathrm{r}}^{2\omega} + I^{2\omega} + 2\alpha\sqrt{I_{\mathrm{r}}^{2\omega} I^{2\omega}} \cos\left(\frac{2\pi l}{L(\omega)} + \Phi_{\mathrm{rs}}\right), \qquad (7)$$

where the period $L(\omega) = \lambda_{\omega}(2\Delta n)^{-1}$ depends on air dispersion at the fundamental and SH wavelength, $\Delta n = n_{2\omega} - n_{\omega}$. The contrast of interference patterns is a function of SH intensities from the sample, $I^{2\omega}$, and reference, $I_{\mathrm{r}}^{2\omega}$, and of the laser-beam coherency, $\alpha < 1$. The relative SH phase of the sample with respect to the reference, Φ_{rs}, can be extracted from the fit of (7) to the experimental SHG interferogram.

The (phase-) reference sample chosen (i) is thin enough to avoid Maker fringes in the SHG response while tuning the fundamental wavelength, (ii) is optically inactive to keep the polarisation state of the fundamental radiation while transmitting through it and (iii) has no resonance features in the tuning regions of the fundamental and SH waves. A plate of crystalline quartz [14] or a film of poled polymer [15], which are conventionally utilised in phase measurements, could not be used for spectroscopic interferometry because of strong spectral dependence of the SH intensity and phase caused by Maker fringes and the resonances of quadratic susceptibility in the experimental spectral range. Therefore a 30-nm-thick indium tin oxide (ITO) film evaporated upon a 1-mm-thick plate of fused quartz is chosen as a phase-reference sample. The SH phase spectrum of the ITO film is measured in the

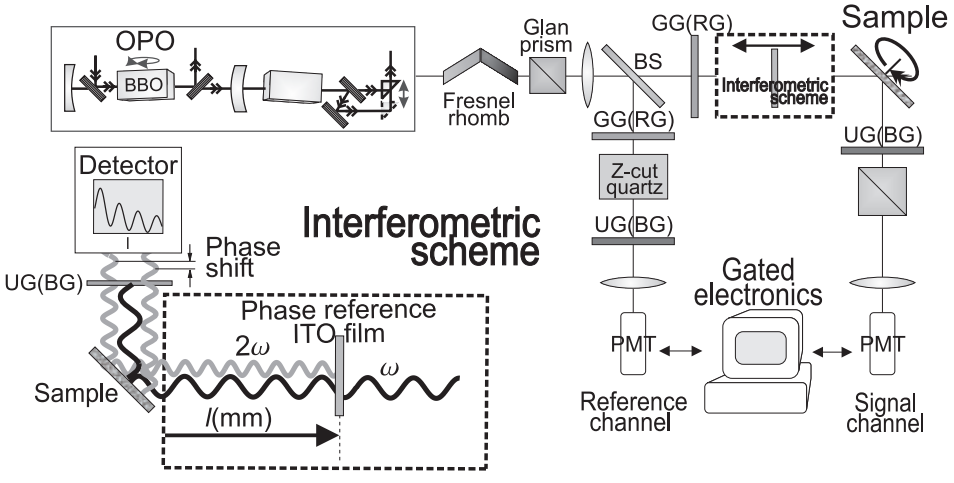

FIGURE 3 Schematic diagram of the experimental setup for combined SH intensity and phase spectroscopy

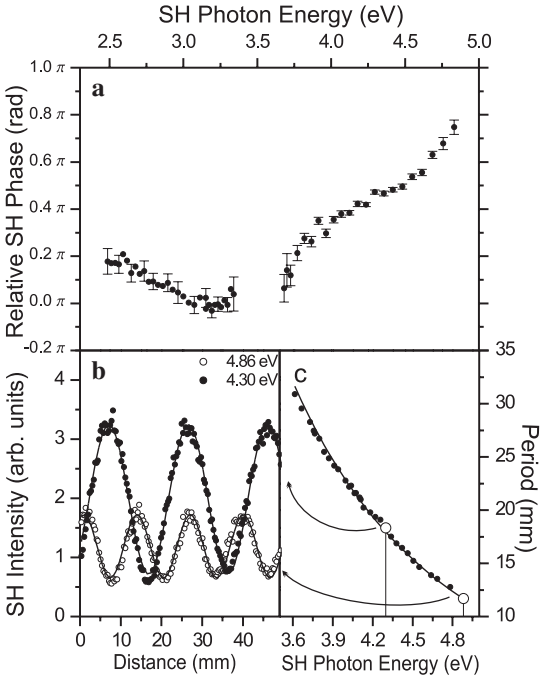

FIGURE 4 **a** The spectrum of the relative phase of the SH field from the ITO (phase-) reference, Φ_{rs}, measured using *y*-cut quartz as a sample. **b** Typical SHG interferograms measured at several SH photon energies. The *curves* are the fits of (7) to data. **c** The spectral dependence of the interference-pattern period and the period spectrum calculated using air-dispersion data from [16]

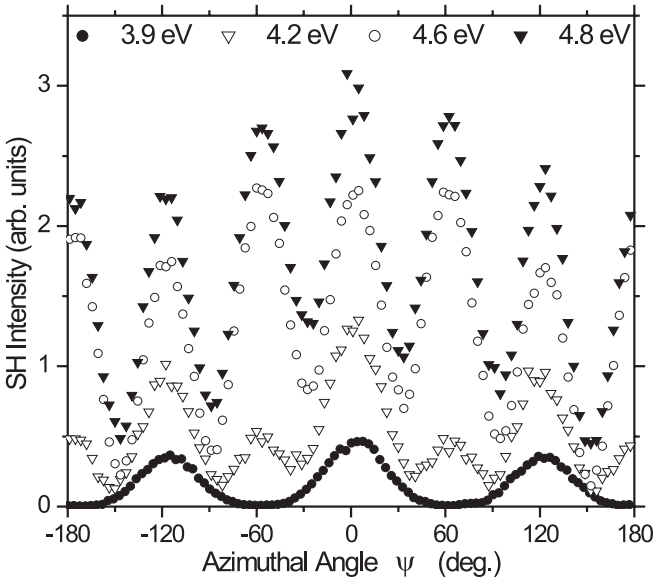

FIGURE 5 SHG anisotropic dependences at a Ge (111)–GeO_2 interface for several SH photon energies

scheme of 'absolute phase measurements' using a backside-immersed plate of *y*-cut quartz as a sample. The phase of the SH wave from the quartz surface is spectrally independent in the whole spectral region. Figure 4b shows typical SHG interference patterns measured for different SH energies. A spectral dependence of the interferogram period due to air dispersion is seen in Fig. 4c. The SH phase spectrum for ITO is shown in Fig. 4a. It has a monotonic spectral dependence and can be easily taken into account. For SH intensity spectral measurements, the ITO film is removed from the setup.

The samples are (i) an optically polished 1-mm-thick *p*-type silicon (111) wafer with resistivity of 2–2.5 Ω cm covered with native oxide and (ii) an optically polished 0.5-mm-thick *n*-type germanium (111) wafer with resistivity of 2.6–3 Ω cm covered with native oxide.

4 Results and discussion

Figure 5 shows a series of azimuthal anisotropic dependences of SH intensity measured at a Ge (111)–GeO_2 interface for several SH photon energies. The symmetry of the curves changes strongly, but monotonically with the spectra, from six-fold at the blue edge of the spectral region used (close to 5 eV) to three-fold at the SH energies close to 3.5 eV. Such a pronounced spectral dependence of the SHG azimuthal anisotropy of the Ge (111) surface is attributed to the strong spectral dependence of the relative phase ϕ between isotropic, C_0, and anisotropic three-fold, $C_3 e^{i\phi} \cos 3\psi$, components of the SH field. In the vicinity of 5 eV, ϕ is close to $\pi/2$, while tuning the SH energy to 3.5 eV leads to a decrease of ϕ to almost zero. A slight one-fold symmetry of anisotropic dependences is apparently associated with a small miscut of the Ge wafer. For a Si (111)–SiO_2 interface, SHG azimuthal dependences possess a three-fold symmetry for the whole spectral range from 3.5 eV to 5 eV, having three large and three small maxima shifted from each other at 60°. All the SH intensity and phase spectra presented below are measured at an azimuthal position shifted by 30° from the large SHG maxima. At this azimuthal angle only the isotropic SHG component C_0 contributes to the azimuthal dependence.

Figure 6 shows spectra of SH intensity and phase measured at a Ge (111)–GeO_2 interface. The SH intensity spectrum has a pronounced step-like feature around 4.3 eV and then the SH intensity strongly increases at the blue edge of the spectrum. The SH phase increases almost monotonically through the whole range by approximately 1.5 radians. The SH intensity spectrum of a Si (111)–SiO_2 interface represented in Fig. 7 has a strong forked peak in the centre of the spectrum. At the edges the SH intensity starts to grow. The SH phase shown in the bottom panel of Fig. 7 increases approximately by 1.2 radians within the interval 4.2 eV to 4.7 eV and has a nonmonotonic feature between 3.6 eV and 4.2 eV.

Experimental SH intensity and phase spectra have been approximated using (4) with $\cos 3\psi = 0$. The effective quadratic susceptibilities, $\chi_{\parallel}^{(2)}$ and $\chi_{\perp}^{(2)}$, in the form of (6) are the superpositions of resonant contributions from several CPs of Si or Ge band structures. This implies that the band-structure modification at the semiconductor surface, and thus the changes of the $\hat{\chi}^{(2),S}$ line shapes, are excluded from the discussion since it requires microscopic ab initio calculations similar to what has been done in [20–22].

For the Ge (111) surface, three resonant contributions are included in the approximation. The first has its central energy in the vicinity of 4.3 eV and is associated with direct transitions at the E_2 CP of the Ge band structure [23]. The second has its central energy around 4.8 eV and is attributed to the resonance of the fundamental radiation with electron transitions

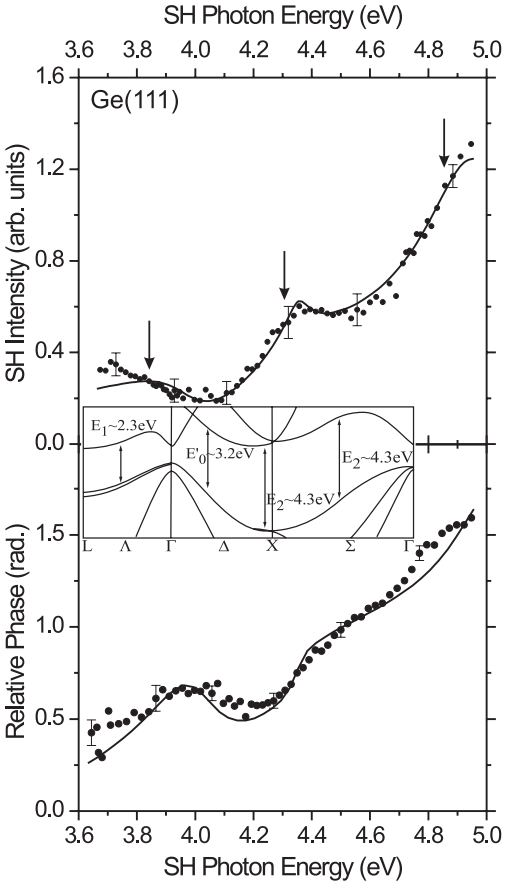

FIGURE 6 SH intensity (*top*) and phase (*bottom*) spectra measured at a Ge(111)–GeO_2 interface in an intermediate position of rotational anisotropy. The *solid curves* represent the result of the combined fit using (4) to experimental spectra obtained for three SHG resonances with central energies $\omega_1 = 3.85$ eV, $\omega_2 = 4.3$ eV and $\omega_3 = 4.85$ eV. *Inset*: the part of the Ge band structure [17] with transition energies taken from [18]

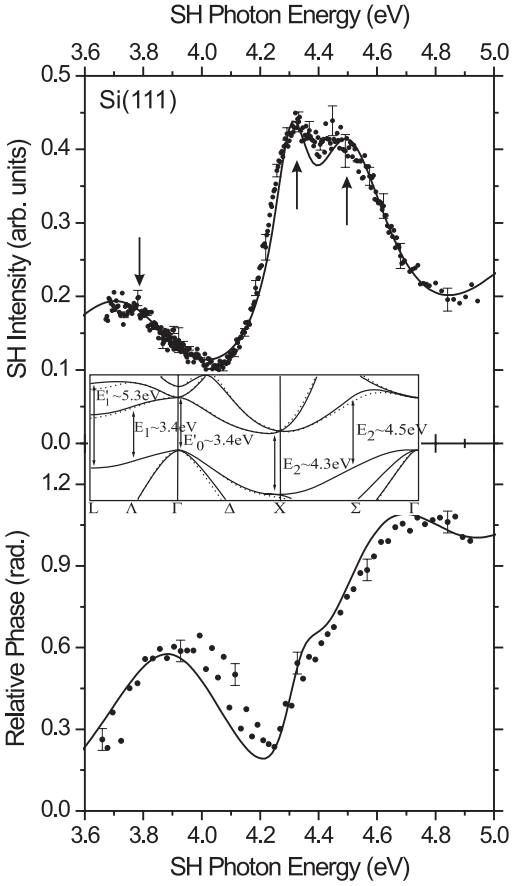

FIGURE 7 SH intensity (*top*) and phase (*bottom*) spectra measured at a Si(111)–SiO_2 interface. The *solid curves* represent the result of the combined fit using (4) to experimental spectra obtained for four SHG resonances with excitonic line shapes and central energies $\omega_1 = 3.8$ eV, $\omega_2 = 4.3$ eV, $\omega_3 = 4.45$ eV and $\omega_4 = 5.2$ eV. *Inset*: the part of the Si band structure from [17] with transition energies taken from [19]

at the lowest-lying E_1 critical point. For both resonances the 2D minimum line shape is taken, in accordance with the critical behaviour of the linear susceptibility at these CPs [18]. The third resonance with an excitonic line shape is located in the low-energy region of the spectra. It is taken to effectively account for the influence of out-of-range SHG resonances located in between the tuning ranges of the fundamental and SH radiation, namely resonances at E_0' and $E_0' + \Delta'$ CPs with central energies in the 2.8-eV to 3.3-eV interval. The solid curves in Fig. 6 show the result of the fit to the SH intensity spectrum simultaneously with the spectral dependence of the SH phase using the least-square procedure with appropriate weights for each spectrum. The curves demonstrate good agreement with the experimental data.

For the Si (111) surface four SHG resonances are taken into account. Two central resonances with energies near 4.3 eV and 4.45 eV can be attributed to $E_2(X)$ and $E_2(\Sigma)$ CPs, respectively [23]. Note that the $E_2(\Sigma)$ resonance is significant in the SHG spectra, whereas it is weak in linear investigations [19]. The resonance at approximately 5.2 eV (out-of-range) more likely corresponds to the E_1' CP. This resonance is included to account for the SH intensity increase and the SH phase inflection at the high-energy edge of the spectra. The last resonance located below 4.0 eV is necessary to approximate a shoulder in the SH intensity spectrum below 4 eV and a nonmonotonic feature in the SH phase spectrum between 3.6 eV and 4.2 eV. The resonant energy 3.8 eV obtained from the combined fit of the SHG spectra has no analogue in linear spectral investigations of silicon. The closest resonances known are the E_0'/E_1 critical point with a central energy of 3.4 eV and the E_0 CP at approximately 4 eV, which is very weak in linear response [23]. The SHG resonance at a nearby energy was recently reported [24] and was attributed to electron transitions in surface Si layers. Solid curves in Fig. 7 represent the fit to experimental data using excitonic line shapes for all resonances. Note that comparable agreement with experimental spectra can also be achieved using 2D line shapes for the quadratic susceptibility in the spectral vicinity of $E_2(X, \Sigma)$ and E_1' CPs, i.e. the same line shapes as for the linear susceptibility [19]. However, the problem of preferable line shapes for $\chi^{(2)}$ of a Si (111) surface in the vicinity of $E_2(X, \Sigma)$ is outside the scope of this paper and will be discussed in more detail in a forthcoming publication [25].

5 Conclusions

In summary, the modification of the second-harmonic phase-measurement technique, that is combined

second-harmonic intensity and phase spectroscopy, is proposed as a spectroscopic probe of the resonant nonlinear optical response of semiconductor surfaces with interfering second-harmonic contributions from nearby electronic resonances. The combination of the spectra of two SH field characteristics – amplitude (intensity) and phase – which are independent combinations of resonant parameters, allows us to derive critical-point parameters and $\chi^{(2)}$ line shapes more accurately. This technique is applied to study the spectroscopic SHG response of Ge (111)–GeO_2 and Si (111)–SiO_2 interfaces in the 3.5-eV to 5-eV SH photon energy interval, where several resonant SHG contributions associated with Van Hove singularities of Ge and Si band structures interfere. For the Ge (111)–GeO_2 interface the contributions from the one-photon resonance of direct transitions near the E_1 CP at the fundamental wavelength and from the two-photon resonance at the E_2 CP are resolved. For the Si (111)–SiO_2 interface, the interference of nearby resonant SHG contributions of the $E_2(X)$ and $E_2(\Sigma)$ critical points is studied. Additional E_1' out-of-range resonance is obtained at the blue edge of the SHG spectrum.

ACKNOWLEDGEMENTS The authors are pleased to acknowledge S. Soria for helpful discussions. This work was supported by the Russian Foundation for Basic Research (RFBR) and the Deutsche Forschungsgemeinschaft (DFG): DFG Grant No. 436 RUS 113/640/0-1, RFBR Grant Nos. 01-02-04018, 01-02-16746 and 01-02-17524, Special Grant for Leading Russian Science Schools No. 00-15-96555 and INTAS Grant No. YSF-2001/1-160.

Appendix

Below, the expressions for the anisotropic SH field reflected from the (111) surface of cubic semiconductors of $m3m$ symmetry are derived for p-in p-out geometry, taking into account complex Green's function corrections for both bulk quadrupole and surface quadratic polarisations. The coordinate systems used in the transformation are shown in Fig. 1. The z axis is directed into the medium. The surface frame is labelled Σ and the crystallographic one is labelled Ω. The variables related to the laboratory frame are not labelled. Both bulk quadrupole and surface terms are considered simultaneously.

The fundamental field amplitude under the surface in the laboratory frame can be expressed as follows:

$$E_{2p}(z,\omega) = T_\omega E_p \mathrm{e}^{\mathrm{i}k_{2z}^{\omega} z}, \tag{A.1}$$

where E_p is the amplitude and T_ω is the Fresnel transmission coefficient for the p-polarised incident wave. Here and below subscript 2 denotes the quantities defined inside the semiconductor while 1 is chosen to label the linear medium (air or oxide). The vector of the fundamental field in the medium can be written as follows:

$$\boldsymbol{E}_2(z,\omega) = E_{2p}(z,\omega)\begin{pmatrix} k_{2z}^{\omega}/k_2^{\omega} \\ 0 \\ k_x^{\omega}/k_2^{\omega} \end{pmatrix}. \tag{A.2}$$

To obtain the SH surface and bulk quadrupole polarisation vectors, $\boldsymbol{k}_2^{\omega}$ and $\boldsymbol{E}_2$ should be transformed to the surface and crystallographic frames, respectively:

$$\boldsymbol{E}_2^{\Sigma}(z,\omega) = \begin{pmatrix} E_{2x}\cos\psi + E_{2y}\sin\psi \\ -E_{2x}\sin\psi + E_{2y}\cos\psi \\ E_{2z} \end{pmatrix}, \tag{A.3}$$

$$\boldsymbol{k}_2^{\omega,\Sigma} = \begin{pmatrix} k_x\cos\psi + k_{2y}\sin\psi \\ -k_x\sin\psi + k_{2y}\cos\psi \\ k_{2z} \end{pmatrix} \tag{A.4}$$

and

$$\boldsymbol{E}_2^{\Omega}(z,\omega) = \frac{1}{\sqrt{6}}\begin{pmatrix} E_{2x} - \sqrt{3}E_{2y} + \sqrt{2}E_{2z} \\ E_{2x} + \sqrt{3}E_{2y} + \sqrt{2}E_{2z} \\ -2E_{2x} + \sqrt{2}E_{2z} \end{pmatrix}^{\Sigma}, \tag{A.5}$$

$$\boldsymbol{k}_2^{\omega,\Omega} = \frac{1}{\sqrt{6}}\begin{pmatrix} k_x - \sqrt{3}k_{2y} + \sqrt{2}k_{2z} \\ k_x + \sqrt{3}k_{2y} + \sqrt{2}k_{2z} \\ -2k_x + \sqrt{2}k_{2z} \end{pmatrix}^{\Sigma}, \tag{A.6}$$

where superscript Σ relates to all quantities inside the brackets.

The nonzero tensor elements of the effective surface quadratic susceptibility of the (111) face of $m3m$ cubic crystals in the surface frame are well known:

$$\begin{aligned} \chi_1^{\mathrm{S}} &= \chi_{xxx} = -\chi_{xyy} = -\chi_{yxy}, \\ \chi_2^{\mathrm{S}} &= \chi_{xzx} = \chi_{yzy}, \\ \chi_3^{\mathrm{S}} &= \chi_{zxx} = \chi_{zyy}, \\ \chi_4^{\mathrm{S}} &= \chi_{zzz}. \end{aligned} \tag{A.7}$$

The nonzero elements of the bulk quadrupole susceptibility in the crystallographic frame are the following:

$$\begin{aligned} \chi_1^{\mathrm{Q}} &= \chi_{xxxx} = \chi_{yyyy} = \chi_{zzzz}, \\ \chi_2^{\mathrm{Q}} &= \chi_{xxzz} = \chi_{yyzz} = \chi_{zzyy} = \chi_{zzxx} = \chi_{xxyy} = \chi_{yyxx}, \\ \chi_3^{\mathrm{Q}} &= \chi_{xzxz} = \chi_{yzyz} = \chi_{zyzy} = \chi_{zxzx} = \chi_{yxyx} = \chi_{xyxy}. \end{aligned} \tag{A.8}$$

This allows us to find the surface and bulk quadratic polarisations in the corresponding frames:

$$\boldsymbol{P}^{\mathrm{S},\Sigma}(z=+0,2\omega) = \hat{\chi}^{(2),\mathrm{S}}(2\omega,\omega,\omega) : \boldsymbol{E}_2^{\Sigma}(\omega)\boldsymbol{E}_2^{\Sigma}(\omega), \tag{A.9}$$

$$\boldsymbol{P}^{\mathrm{Q},\Omega}(z,2\omega) = \hat{\chi}^{(2),\mathrm{Q}}(2\omega,\omega,0,\omega) : \boldsymbol{E}_2^{\Omega}(z,\omega)\nabla\boldsymbol{E}_2^{\Omega}(z,\omega). \tag{A.10}$$

The left-hand vectors expressed in the components are:

$$\boldsymbol{P}^{\mathrm{S},\Sigma} = \begin{pmatrix} \chi_1^{\mathrm{S}}(E_{2x}^2 - E_{2y}^2) + 2\chi_2^{\mathrm{S}}E_{2z}E_{2x} \\ -2\chi_1^{\mathrm{S}}E_{2x}E_{2y} + 2\chi_2^{\mathrm{S}}E_{2z}E_{2y} \\ \chi_3^{\mathrm{S}}(E_{2x}^2 + E_{2y}^2) + \chi_4^{\mathrm{S}}E_{2z}^2 \end{pmatrix}^{\Sigma}, \tag{A.11}$$

$$
\begin{aligned}
P_x^{\mathrm{Q},\Omega} &= \mathrm{i}\Big(\chi_1^{\mathrm{Q}} k_x E_{2x}^2 + 2\chi_2^{\mathrm{Q}} E_{2x} \\
&\quad \times (k_{2z}E_{2z} + k_{2y}E_{2y}) + \chi_3^{\mathrm{Q}} k_x (E_{2z}^2 + E_{2y}^2)\Big)^{\Omega}, \\
P_y^{\mathrm{Q},\Omega} &= \mathrm{i}\Big(\chi_1^{\mathrm{Q}} k_{2y} E_{2y}^2 + 2\chi_2^{\mathrm{Q}} E_{2y} \\
&\quad \times (k_{2z}E_{2z} + k_x E_{2x}) + \chi_3^{\mathrm{Q}} k_{2y} (E_{2x}^2 + E_{2z}^2)\Big)^{\Omega}, \\
P_z^{\mathrm{Q},\Omega} &= \mathrm{i}\Big(\chi_1^{\mathrm{Q}} k_{2z} E_{2z}^2 + 2\chi_2^{\mathrm{Q}} E_{2z} \\
&\quad \times (k_{2y}E_{2y} + k_x E_{2x}) + \chi_3^{\mathrm{Q}} k_{2z} (E_{2y}^2 + E_{2x}^2)\Big)^{\Omega}.
\end{aligned}
\tag{A.12}
$$

The transformation of the quadrupole SH polarisation to the surface frame is:

$$
\boldsymbol{P}^{\mathrm{Q},\Sigma} = \frac{1}{\sqrt{6}} \begin{pmatrix} P_x + P_y - 2P_z \\ -\sqrt{3}P_x + \sqrt{3}P_y \\ \sqrt{2}P_x + \sqrt{2}P_y + \sqrt{2}P_z \end{pmatrix}^{\Omega}. \tag{A.13}
$$

The transformation of both SH polarisation vectors from the surface frame to the laboratory frame can be done identically:

$$
\boldsymbol{P}^{\mathrm{Q(S)}} = \begin{pmatrix} P_x \cos\psi - P_y \sin\psi \\ P_x \sin\psi + P_y \cos\psi \\ P_z \end{pmatrix}^{\Sigma}. \tag{A.14}
$$

The detected SH intensity and phase are the squared modulus and phase of the SH field obtained by convolution of the SH polarisation vectors with the corresponding Green's function tensor [10]:

$$
\begin{aligned}
&\boldsymbol{E}(-0, 2\omega) \\
&= -4\pi \left(\frac{2\omega}{c}\right)^2 \int_0^{\infty} \hat{G}(-0, z') \cdot [\boldsymbol{P}^{\mathrm{S}} \delta(z' - 0) + \boldsymbol{P}^{\mathrm{Q}}(z')] \mathrm{d}z' \\
&= -4\pi \left(\frac{2\omega}{c}\right)^2 \left[\hat{G}_0 \cdot \boldsymbol{P}^{\mathrm{S}} + \hat{G}_0 \cdot \boldsymbol{P}^{\mathrm{Q}} \int_0^{\infty} \mathrm{e}^{\mathrm{i}\left(k_{2z}^{2\omega} + 2k_{2z}^{\omega}\right) z'} \mathrm{d}z' \right] \\
&= -4\pi \left(\frac{2\omega}{c}\right)^2 \hat{G}_0 \cdot \left[\boldsymbol{P}^{\mathrm{S}} + \frac{\mathrm{i}\boldsymbol{P}^{\mathrm{Q}}}{\Delta} \right],
\end{aligned}
\tag{A.15}
$$

where $\Delta = k_{2z}^{2\omega} + 2k_{2z}^{\omega}$, $\hat{G}_0 = \hat{G}(-0, +0)$, and the Green's function tensor for a semi-infinite medium is [11]:

$$
\hat{G}_{ij}(-0, z') = \alpha(1 - R_p^2) \begin{pmatrix} 1 & \frac{k_x^{2\omega}}{k_{2z}^{2\omega}} \\ \frac{k_x^{2\omega}}{k_{1z}^{2\omega}} & \frac{(k_x^{2\omega})^2}{k_{1z}^{2\omega} k_{2z}^{2\omega}} \end{pmatrix} \mathrm{e}^{\mathrm{i}k_{2z}^{2\omega} z'}, \tag{A.16}
$$

where

$$
\alpha = -\mathrm{i}(\varepsilon_1 k_{2z}^{2\omega} + \varepsilon_2 k_{1z}^{2\omega}) / 4\varepsilon_1 \varepsilon_2 (2\omega/c)^2, \tag{A.17}
$$

$i, j = x, z$, and $R_p = (\varepsilon_1 k_{2z}^{2\omega} - \varepsilon_2 k_{1z}^{2\omega})/(\varepsilon_1 k_{2z}^{2\omega} + \varepsilon_2 k_{1z}^{2\omega})$ is the Fresnel coefficient for reflection of the p-polarised SH wave. After subsequent transformation of vectors $\boldsymbol{P}^{\mathrm{S},\Sigma}$ and $\boldsymbol{P}^{\mathrm{Q},\Omega}$ to the laboratory frame, (A.15) has the form:

$$
\boldsymbol{E}(-0, 2\omega) = G_0 E_p^2 (C_0 + C_3 \cos 3\psi) \begin{pmatrix} 1 \\ 0 \\ k_x^{2\omega}/k_{2z}^{2\omega} \end{pmatrix}, \tag{A.18}
$$

where $G_0 = 2\pi \mathrm{i} k_{2z}^{2\omega} \varepsilon_2^{-1} T_{\omega}^2$. The amplitudes C_0 and C_3 of the Fourier expansion over the azimuthal angle ψ are as follows:

$$
\begin{aligned}
C_0 &= 2\chi_2^{\mathrm{S}} \tfrac{k_x^{\omega} k_{2z}^{\omega}}{(k_2^{\omega})^2} + \tfrac{k_x^{2\omega}}{k_{2z}^{2\omega}} \left(\chi_4^{\mathrm{S}} \tfrac{(k_x^{\omega})^2}{(k_2^{\omega})^2} + \chi_3^{\mathrm{S}} \tfrac{(k_{2z}^{\omega})^2}{(k_2^{\omega})^2} \right) \\
&\quad - \tfrac{1}{6\Delta} \left(k_x^{\omega} \left(2\tilde{\chi}_1 \tfrac{(k_x^{\omega})^2}{(k_2^{\omega})^2} + \tilde{\chi}_2 \tfrac{(k_{2z}^{\omega})^2}{(k_2^{\omega})^2} \right) \right. \\
&\quad \left. + 2k_{2z}^{\omega} \tfrac{k_x^{2\omega}}{k_{2z}^{2\omega}} \left(3\tilde{\chi}_3 \tfrac{(k_x^{\omega})^2}{(k_2^{\omega})^2} + \tilde{\chi}_1 \tfrac{(k_{2z}^{\omega})^2}{(k_2^{\omega})^2} \right) \right), \\
C_3 &= \chi_1^{\mathrm{S}} \tfrac{(k_{2z}^{\omega})^2}{(k_2^{\omega})^2} + \tfrac{\sqrt{2}k_{2z}^{\omega}}{6\Delta} (\tilde{\chi}_2 - 6\tilde{\chi}_3) \\
&\quad \times \left(\tfrac{k_x^{\omega} k_{2z}^{\omega}}{(k_2^{\omega})^2} \tfrac{k_x^{2\omega}}{k_{2z}^{2\omega}} + \tfrac{2(k_x^{\omega})^2 + (k_{2z}^{\omega})^2}{(k_2^{\omega})^2} \right),
\end{aligned}
\tag{A.19}
$$

where $\tilde{\chi}_1$, $\tilde{\chi}_2$ and $\tilde{\chi}_3$ collect the following combinations of quadrupole susceptibility components:

$$
\begin{aligned}
\tilde{\chi}_1 &= \chi_1^{\mathrm{Q}} - 2\chi_2^{\mathrm{Q}} + 2\chi_3^{\mathrm{Q}}, \\
\tilde{\chi}_2 &= 7\chi_1^{\mathrm{Q}} + 10\chi_2^{\mathrm{Q}} - \chi_3^{\mathrm{Q}}, \\
\tilde{\chi}_3 &= \chi_1^{\mathrm{Q}} + 2\chi_2^{\mathrm{Q}}.
\end{aligned}
\tag{A.20}
$$

REFERENCES

1 For a review, see G. Lüpke: Surf. Sci. Rep. **35**, 75 (1999)
2 W. Daum, H.-J. Krause, U. Reichel, H. Ibach: Phys. Rev. Lett. **71**, 1234 (1993)
3 C. Meyer, G. Lüpke, U. Emmerichs, F. Wolter, H. Kurz, C.H. Bjorkman, G. Lucovsky: Phys. Rev. Lett. **74**, 3001 (1995)
4 P.T. Wilson, Y. Jiang, O.A. Aktsipetrov, E.D. Mishina, M.C. Downer: Opt. Lett. **24**, 496 (1999)
5 G. Erley, R. Butz, W. Daum: Phys. Rev. B **59**, 2915 (1999)
6 T.F. Heinz, F.J. Himpsel, E. Palange, E. Burstein: Phys. Rev. Lett. **63**, 644 (1989)
7 O.A. Aktsipetrov, A.A. Fedyanin, A.V. Melnikov, E.D. Mishina, A.N. Rubtsov, M.H. Anderson, P.T. Wilson, M. ter Beek, X.F. Hu, J.I. Dadap, M.C. Downer: Phys. Rev. B **60**, 8924 (1999)
8 O.A. Aktsipetrov, I.M. Baranova, Yu.A. Il'inskii: Sov. Phys. JETP **64**, 167 (1986) [Zh. Exsp. Teor. Fiz. **91**, 287 (1986)]
9 J.E. Sipe, D.J. Moss, H.M. van Driel: Phys. Rev. B **35**, 1129 (1987)
10 P. Guyot-Sionnest, W. Chen, Y.R. Shen: Phys. Rev. B **33**, 8254 (1986)
11 A. Bagchi, R.G. Barrera, A.K. Rajogopal: Phys. Rev. B **20**, 771 (1979)
12 D.E. Aspnes, A.A. Studna: Phys. Rev. B **27**, 985 (1983)
13 M. Cardona: *Modulation Spectroscopy*, Suppl. 11 of *Solid State Physics*, ed. by F. Seitz, D. Turnbull, H. Ehrenreich (Academic, New York 1969) Chapt. 2
14 K. Kemnitz, K. Bhattacharyya, J.M. Hicks, G.R. Pinto, K.B. Eisenthal, T.F. Heinz: Chem. Phys. Lett. **131**, 285 (1986)
15 R. Stolle, G. Marowsky, E. Schwarzberg, G. Berkovic: Appl. Phys. B **63**, 491 (1996)
16 B. Edlen: Metrologia **2**, 71 (1966)
17 J.R. Chelikowsky, M.L. Cohen: Phys. Rev. B **14**, 556 (1976)
18 L. Vina, S. Logothetidis, M. Cardona: Phys. Rev. B **30**, 1979 (1984)
19 P. Lautenschlager, M. Garriga, L. Vina, M. Cardona: Phys. Rev. B **36**, 4821 (1987)
20 S. Hollemann, F. Rebentrost: Surf. Sci. **331–333**, 1342 (1995)
21 B.S. Mendoza, A. Gaggiotti, R. Del Sole: Phys. Rev. Lett. **81**, 3781 (1998)
22 V.I. Gavrilenko, R.Q. Wu, M.C. Downer, J.G. Ekerdt, D. Lin, P. Parkinson: Phys. Rev. B **63**, 165 325 (2001)
23 O. Madelung, M. Schulz, H. Weiss (eds.): *Semiconductors, Landolt-Börnstein,* Vol. 17a, 17b (Springer, Berlin 1982)
24 G. Erley, W. Daum: Phys. Rev. B **58**, R1734 (1998)
25 T.V. Dolgova, A.A. Fedyanin, O.A. Aktsipetrov, G. Marowsky: Phys. Rev. B **65**(27), (2002) in print